Western Pacific coastal sources of iron, manganese, and aluminum to the Equatorial Undercurrent

Lia O. Slemons,[1] James W. Murray,[1] Joseph Resing,[2] Barbara Paul,[1] and Pierre Dutrieux[3,4]

Received 16 October 2009; revised 22 March 2010; accepted 26 April 2010; published 22 September 2010.

[1] We present results from the first zonal transect of iron, aluminum, and manganese conducted from the western source region of the Equatorial Undercurrent (EUC) to the central equatorial Pacific. Trace metals were elevated along the slope of Papua New Guinea and within the New Guinea Coastal Undercurrent (NGCU), which is the primary Southern Hemisphere entry path of water to the EUC. Subsurface maxima in total acid-soluble iron, aluminum, and manganese were evident in the EUC. These maxima were generally greatest in the western equatorial Pacific and decreased in magnitude eastward. Maxima in iron and aluminum persisted to 140°W; maxima in manganese extended to 175°W. Iron and manganese maxima were deeper (25–75 m) than aluminum maxima and located in the lower EUC, which undergoes less interior ocean mixing than shallower waters. The depth of the aluminum subsurface maxima correlated strongly ($r = 0.88$) with the depth of the EUC velocity maximum. Surface waters were enriched in aluminum and manganese offshore of Papua New Guinea. Surface metal concentrations decreased eastward throughout the western warm pool up to the longitude (~180°W) of the salinity front. Detrital sediment input from either direct riverine input or sediment resuspension appeared to be the primary mechanism of supplying metals to the NGCU. We estimated eastward fluxes of metals in the EUC and found greatest fluxes in the western equatorial Pacific between 160°E and 165°E, except for aluminum. Fluxes of aluminum and, to a lesser extent, manganese increased concurrently with water volume transport in the central equatorial Pacific. Iron transport in the EUC remained constant east of the dateline, apparently due to the combined effects of dilution by meridional entrainment and scavenging. Iron was mobilized in a highly active western boundary current region and transported eastward in the lower EUC.

Citation: Slemons, L. O., J. W. Murray, J. Resing, B. Paul, and P. Dutrieux (2010), Western Pacific coastal sources of iron, manganese, and aluminum to the Equatorial Undercurrent, *Global Biogeochem. Cycles*, *24*, GB3024, doi:10.1029/2009GB003693.

1. Introduction

1.1. Water Mass Crossroads in the Formation Region of the Equatorial Undercurrent

[2] One of the ocean's largest high nitrate-low chlorophyll (HNLC) regions is fuelled by nutrient-rich water from the Equatorial Undercurrent (EUC) [*Murray et al.*, 1994] that reaches the surface in the eastern equatorial Pacific Ocean. The EUC originates in the western equatorial Pacific, at a "water mass crossroads" [*Fine et al.*, 1994], where thermocline and intermediate waters formed in both hemispheres meet at densities between σ_θ = 24.5–26.6 kg m^3 (corresponding to 120–320 m depth) and flow eastward, bringing to the surface cold, nutrient- and CO_2-rich water in the HNLC eastern equatorial Pacific [*Tsuchiya et al.*, 1989; *Johnson et al.*, 2002]. The velocity core of the EUC is centered in the thermocline and is associated with a tongue of high-salinity water originating from South Pacific tropical water [*Tsuchiya et al.*, 1989]. The majority of EUC water transport occurs in the lower thermocline, known as the 13°C water, although the average zonal current is less than in the central thermocline [*Tsuchiya et al.*, 1989]. An important difference between the deeper and shallower EUC waters in the eastern equatorial Pacific is the dominance of the western boundary currents as a source of the deeper 13°C water, while the shallower thermocline waters have undergone more mixing and entrainment of interior waters in subtropical cells

[1]School of Oceanography, University of Washington, Seattle, Washington, USA.
[2]Pacific Marine Environmental Laboratory, National Oceanic Atmospheric Administration, Seattle, Washington, USA.
[3]School of Ocean and Earth Science and Technology, University of Hawaii, Honolulu, Hawaii, USA.
[4]Now at Physical Science Division, British Antarctic Survey, Cambridge, UK.

0886-6236/10/2009GB003693

[*Johnson and McPhaden*, 1999; *Fukumori et al.*, 2004; *Qu et al.*, 2009].

[3] At the surface, west to east gradients of salinity, temperature, pCO_2, and macronutrients delineate the western warm, fresh pool from the cold, salty tongue [*Philander*, 1990; *Murray et al.*, 1994; *Stoens et al.*, 1999; *Johnson et al.*, 2002; *Le Borgne et al.*, 2002; *Sloyan et al.*, 2003]. In the central equatorial Pacific, mixing of surface and upper thermocline waters is driven by local wind stress and heat flux from tropical instability waves [*Menkes et al.*, 2006; *Dutrieux et al.*, 2008]. Surface equatorial divergence forms the poleward leg of subtropical recirculation cells [*Lu et al.*, 1998] that downwell and recirculate half of their water mass within 8° of the equator [*Johnson*, 2001].

[4] The far western equatorial Pacific, bordered by the islands of the Bismarck Archipelago and Papua New Guinea, is the crossroads for equatorward low-latitude western boundary currents (LLWBCs) that scour the steep submarine slopes of the surrounding mountainous volcanic islands [*Tsuchiya et al.*, 1989; *Butt and Lindstrom*, 1994]: the Mindanao Current north of the equator and the New Guinea and New Ireland Coastal Undercurrents (NGCU and NICU) in the south. The NGCU provides roughly 3 times the water volume of the NICU to the EUC [*Butt and Lindstrom*, 1994]. The NGCU flows northwestward along the Papua New Guinea slope and partially retroflects to join the EUC [*Fine et al.*, 1994; *Sloyan et al.*, 2003]. The NICU feeds the EUC east of 149°E [*Butt and Lindstrom*, 1994].

1.2. Role of Continental Iron Sources

[5] Continental margin sediments are increasingly recognized as important sources of iron (Fe) to the open ocean in the central [*Elrod et al.*, 2004], North Pacific [*Lam et al.*, 2006; *Lam and Bishop*, 2008; *Chase et al.*, 2007; *Nishioka et al.*, 2007; *Cullen et al.*, 2009], and North Atlantic oceans [*Laës et al.*, 2007]. Few global biogeochemical models include sedimentary Fe sources, although a recent global simulation suggests that sedimentary sources are almost equal to atmospheric sources of Fe in the ocean [*Moore and Braucher*, 2008]. In addition to sedimentary fluxes, riverine fluxes of particulate matter from the New Guinea platform are especially large [*Milliman et al.*, 1999; *Sholkovitz et al.*, 1999] and can be transported across the slope over great distances via isopycnal plumes and hyperpycnal flows [*Kineke et al.*, 2000; *Kuehl et al.*, 2004]. Maxima in particulate Fe, Mn, and Al and dissolved Fe at 140°W at the base of the equatorial thermocline led *Gordon et al.* [1997] to propose a lithogenic iron source from the New Guinea platform. Trace metal measurements of total acid-soluble Fe, Mn, Cd, Cu, and Ni offshore of Papua New Guinea and in the western equatorial Pacific to 155°E were conducted by *Mackey et al.* [2002a; 2002b]. On the basis of their observations of large Mn and Fe enrichments (that did not vary with ENSO and its associated variable river runoff) and layers with high total suspended matter indicative of sediment injection at depths down to 450 m offshore of Papua New Guinea, they proposed that sediments are the origin of metals to the EUC via the NGCU [*Mackey et al.* 2002a; 2002b]. Boundary exchange with the steep-sided islands traversed by these currents imparts an island weathering signature that has been measured in the western and central equatorial Pacific [*Sholkovitz et al.*, 1999; *Lacan and Jeandel*, 2001].

[6] Here we present results from a transect from Vitiaz Strait, the entry point of the NGCU into the Bismarck Sea, along and beyond the northeast coast of Papua New Guinea to 2°N, 145°E and a zonal transect from 145°E to 140°W along the equator. The aims of this study were to (1) determine whether there was a source of Fe, Al, and/or Mn from the western equatorial Pacific to the EUC; (2) measure the zonal gradient of these metals along the EUC and associated waters; and (3) describe plausible mechanisms for such a source.

2. Methods

2.1. Sample Collection and Treatment

[7] We collected samples from the surface to 1000 m with high resolution (every 25 m between 75 and 250 m) in the thermocline aboard the R/V *Kilo Moana* cruise 0625 (http://www.ocean.washington.edu/cruises/KiloMoana2006/index.html) from Honolulu, HI, to Rabaul, Papua New Guinea, in August/September 2006 (Figure 1). The Southern Hemisphere source region for the EUC was sampled off the steep continental slope of Papua New Guinea, including upstream (station 29) and downstream (station 28) of the Sepik River, the largest river on the northeast coast of Papua New Guinea, and in Vitiaz Strait (station 30), the narrow (50 km) entry point of water from the Solomon Sea [*Tsuchiya et al.*, 1989; *Fine et al.*, 1994].

[8] Seawater was collected in twelve 10 L Teflon-lined GO-FLO bottles (General Oceanics) that were gently cleaned with detergent following established protocols [*Measures et al.*, 2008a] and were then repeatedly filled with open-ocean seawater during the 5 day transit from Honolulu, HI, to station 1. Bottles were mounted on a newly powder-coated rosette frame shortly prior to deployment. Vectran cable spooled on a plastic-sheathed drum and level wound by hand was employed for all trace metal casts. Standard oceanographic data were measured with conductivity-temperature-depth (CTD) sensors (SeaBird SBE 911).

[9] Immediately upon recovery, GO-FLO bottles were transferred to a plastic-lined enclosure constructed within an aft shipboard laboratory and mounted on painted wooden wall-mounted racks for sampling. Iron samples were collected and stored in low-density polyethylene bottles, which had been filled with 0.01 *M* Q-HCl after sequential cleaning in Micro™-detergent solution (1 week at room temperature), and 3 *M* HCl and then 4 *M* HNO_3 (both overnight at 60°C) with thorough intermediate rinsing with 18 Ω deionized water between each cleaning. Aluminum samples were collected in polymethyl pentane bottles that had been stored in 0.05 *M* subboiling distilled HCl after being cleaned in 10% HCl at 60°C for 24 h followed by thorough and immediate rinsing with 18 Ω deionized water. Manganese samples were collected in commercially precleaned I-Chem bottles, which had been stored with 0.05 *M* subboiling distilled HCl for >2 months. Total acid-soluble (abbreviated as TD, total dissolvable, following *Mackey et al.* [2002a]) samples of TDFe, TDMn, and TDAl were collected first. The GO-FLO bottles were connected to a compressed air filtration system, and seawater was filtered through acid-cleaned 0.4 μm Nucleopore

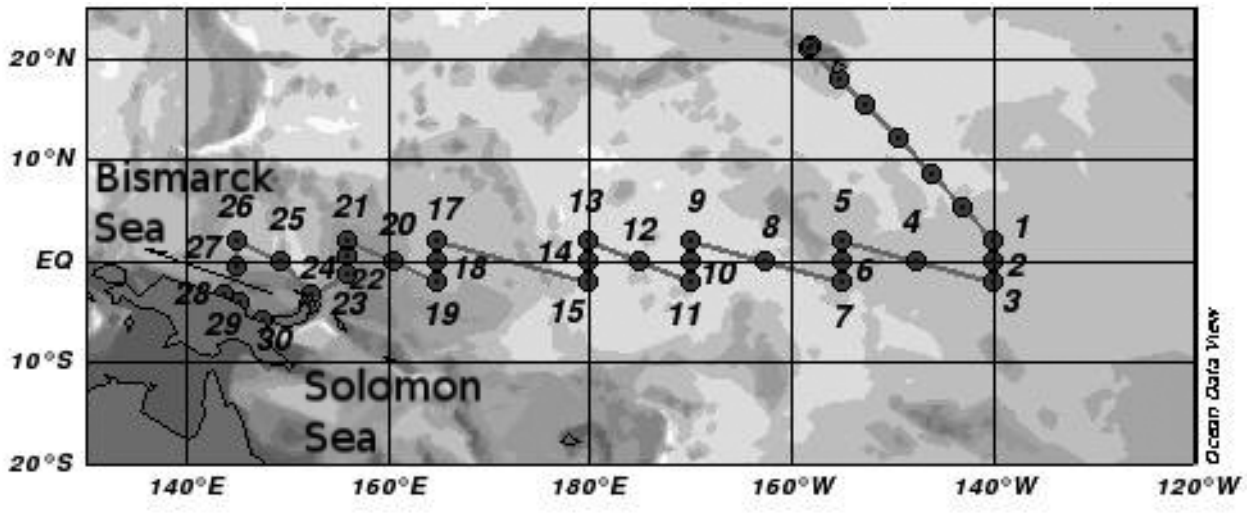

Figure 1. Chart of cruise track for R/V *Kilo Moana* 0625 (EUCFe) with station locations. Line indicates location of Bismarck Sea.

polycarbonate filters to collect dissolved samples (DFe, DMn, and DAl). Filters were flushed with at least 1 L of seawater prior to sample collection. Here we define dissolved metals as those that pass through a 0.4 μm filter although they likely include both a truly soluble and colloidal fraction [e.g., *Wu et al.*, 2001]. The unfiltered measurements yield concentrations that are the total amount of a metal dissolved upon acidification of the sample. All samples were acidified to pH = 1.8 with BASELINE® grade HCl from SEASTAR™ within 4 h of collection and stored at least 24 h prior to analysis.

2.2. Analytical Techniques

[10] Iron was analyzed by flow injection analysis (FIA) using in-line preconcentration with luminol chemiluminescence detection [*Obata et al.*, 1993]. Samples were adjusted to a pH between 3.0 and 3.6 and reoxidized with H_2O_2 prior to analysis, since Fe (III) is retained on the 8-hydroxyquinoline column at this pH range [*Obata et al.*, 1993; our study]. We set up the analytical system as described by *Johnson et al.* [2003]. The detection limit (=3 times the standard deviation of the zero-load-time blank) was 0.05 n*M* for a 4 min sample load time. Precision, on the basis of 10 duplicates from the cruise across a concentration range of 0.35–4 n*M* Fe, was 4.1%, including duplicates measured months apart.

[11] Internal standards were used throughout shipboard and postcruise analysis. Large volume (2 L), triplicate samples of unfiltered surface seawater from the shipboard surface water sampling system, which was designed to minimize trace metal contamination, and one 2 L filtered sample from 175 m were collected at the first station for use as internal standards. The seawater standards were acidified immediately to pH 1.8 in cleaned low-density polyethylene bottles. The average value of the internal standard from 175 m was 0.49 ± 0.09 n*M* or 18% (1 relative standard deviation, n = 19). The internal standard from the shipboard sampling system averaged 1.12 ± 0.17 n*M* or 15% (n = 19). At least one internal standard was measured on each day of sample analysis. Measurements were rejected if the internal standard measurement for that set of samples deviated from the average value by more than 1 relative standard deviation. Our concurrent analyses of the SAFe S1-403 Fe standard with the EUCFe samples yielded a value of 0.12 ± 0.012 n*M*, which is statistically the same as the consensus value of 0.097 ± 0.043 nM.

[12] Aluminum was determined by FIA using in-line preconcentration with fluorescence detection. The limit of detection for Al was 0.15 nM with a precision of 3.5% [*Resing and Measures*, 1994]. Manganese was measured by FIA using in-line preconcentration and spectrophotometric detection [*Resing and Mottl*, 1992]. The limit of detection was 0.050 nM, and precision, on the basis of replicates during the cruise, was 3.0%.

2.3. Acoustic Doppler current profiler and Transmissometry Measurements

[13] The University of Hawaii R/V *Kilo Moana* routinely employs a combination of 300 kHz Work Horse and 38 kHz Ocean Surveyor RD instruments Acoustic Doppler Current Profilers (ADCPs). Measurements from both instruments were individually processed using the UHDAS software (http://currents.soest.hawaii.edu) and binned in 5 m intervals from 30 to 1800 m. Velocity errors were mainly due to poor meteorological conditions or weak acoustic scattering and are expected to be less than 0.04 m s^{-1}. Instantaneous water volume flux estimates were calculated by interpolating velocity measurements onto a regular latitudinal-longitudinal grid. Transmissometry data was recorded using a WetLabs C-Star transmissometer with a 25 cm path length.

3. Results and Discussion

3.1. Local Dynamical Conditions

[14] Sampling occurred during the onset of a mild El Niño, associated with westerly wind bursts in late June and August 2006 [*McPhaden*, 2008]. A strong salinity front characteristic of the eastern boundary of the warm pool was evident at about

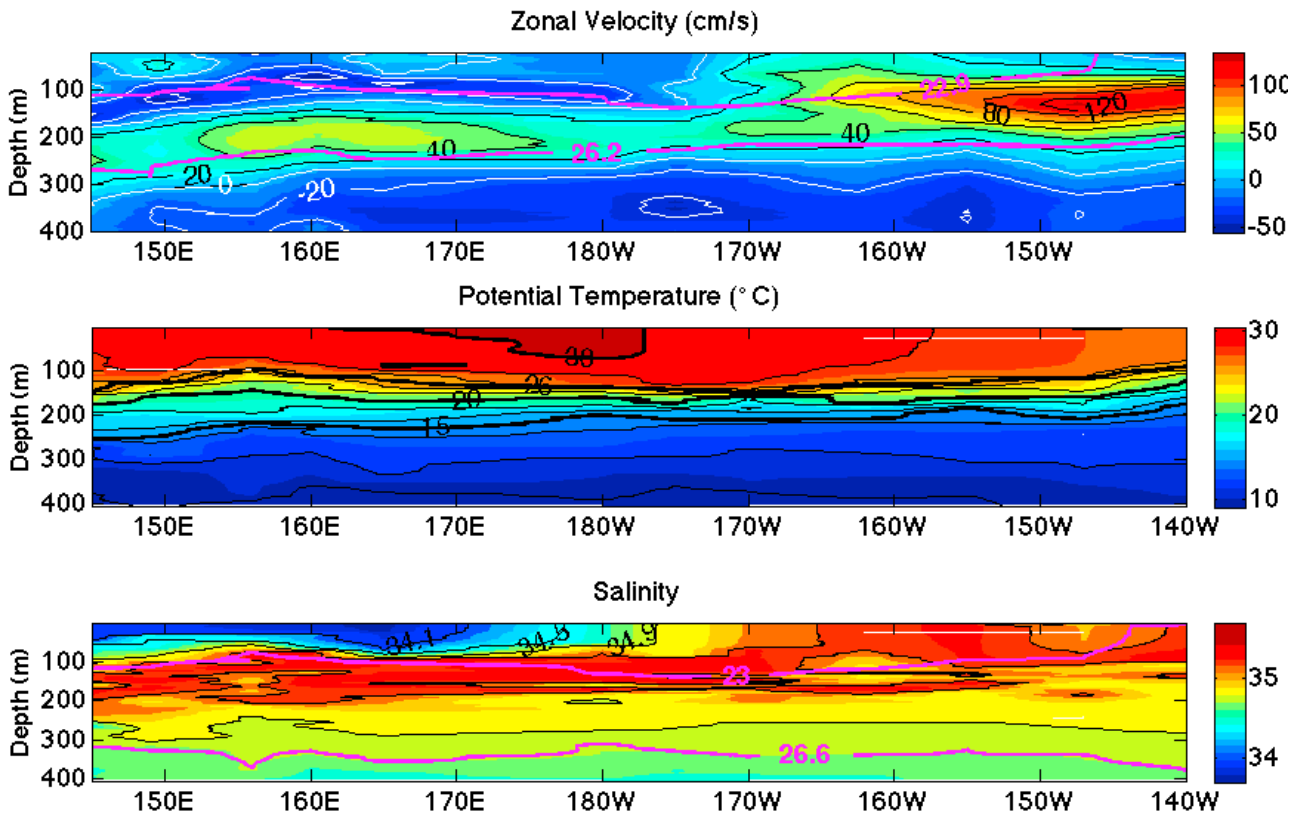

Figure 2. (top) Zonal current (m s^{-1}), (middle) temperature (°C), and (bottom) salinity along the equator from 140°W to 145°E. (top) The density surfaces corresponding to the deepest (σ_θ = 26.2 kg m^{-3}) and shallowest (σ_θ = 22.9 kg m^{-3}) maximum zonal velocities at our equatorial stations are overlain in pink. (top and bottom) EUC at σ_θ = 23.0 and 26.6 kg m^{-3}, respectively, are overlain in pink.

the dateline (Figure 2). ADCP data indicated that the core of the EUC shoaled ~100 m between 180°W and 155°W and was strongest in the central equatorial Pacific between 150°W and 140°W. Cross-slope transects off the islands of Papua New Guinea and New Ireland provided snapshot measurements of the major southern LLWBCs in the region. The transport of the NGCU (4.8 sverdrup (Sv)) could contribute up to 62% of the EUC at 145°E (7.8 Sv) (Figure 3), while at 156°E, the combined transport of the NGCU and NICU (6.1 Sv) contributed up to ~50% of the EUC (12.4 Sv). These contributions are consistent with estimates from tracers, currents, and models that show that Southern Hemisphere LLWBCs provide ~50% to 67% of source water to the EUC [*Tsuchiya et al.*, 1989; *Butt and Lindstrom*, 1994; *Rodgers*, 2003]. The volume of the EUC increases downstream as subtropical water is entrained in the interior Pacific. Most (~3/4) of the additional water is from the Southern Hemisphere, since potential vorticity barriers prevent significant mixing from the Northern Hemisphere [*Johnson and McPhaden*, 1999].

[15] The velocity maximum of the EUC is typically located in the center of the thermocline, nominally at 17°C [*Johnson et al.*, 2002]. During our cruise, the EUC velocity maximum was between σ_θ = 25.6 and 26.2 kg m^{-3} west of 170°W and then underwent an abrupt shoaling between 170°W and 160°W to between σ_θ = 22.9 and 24.3 kg m^{-3} from 162°W to 140°W (Figure 2). We considered the high-velocity, upper EUC to be between the shallowest eastward flowing density deeper than σ_θ = 22.9 kg m^{-3} and σ_θ = 25.8 kg m^{-3}. The lower EUC is a thick (45–105 m during our cruise), homogeneous water mass known as 13°C Water in the eastern equatorial Pacific. It is defined as the depth interval where the vertical temperature gradient is weakest near σ_θ = 26.2–26.4 kg m^{-3} [*Tsuchiya et al.*, 1989; *Qu et al.*, 2009]. We adopted the density range for the lower EUC by *Qu et al.* [2009] from σ_θ = 25.8 kg m^{-3} to the deepest eastward flowing density shallower than σ_θ = 26.6 kg m^{-3}, which ranged between σ_θ = 26.3 and 26.6 kg m^{-3} for our stations. The upper and lower density bounds of the EUC are overlain in Figure 2.

3.2. Western Source Region Profiles

[16] Trace metal concentrations in the low-latitude western boundary current on the northeast margin of Papua New Guinea are shown in Figure 4. NGCU flow was not clearly represented in the underway shipboard velocity measurements. Since South Pacific tropical water is the major source of the maximum in salinity in the southern EUC endmembers [*Tsuchiya et al.*, 1989; *Fine et al.*, 1994], salinity was used as a tracer of NGCU, which suggested a depth between 120 and 320 m, in Figures 4 and 5. Complex patterns of trace metal enrichments were found along this tectonically active, high sediment input margin. These coastal

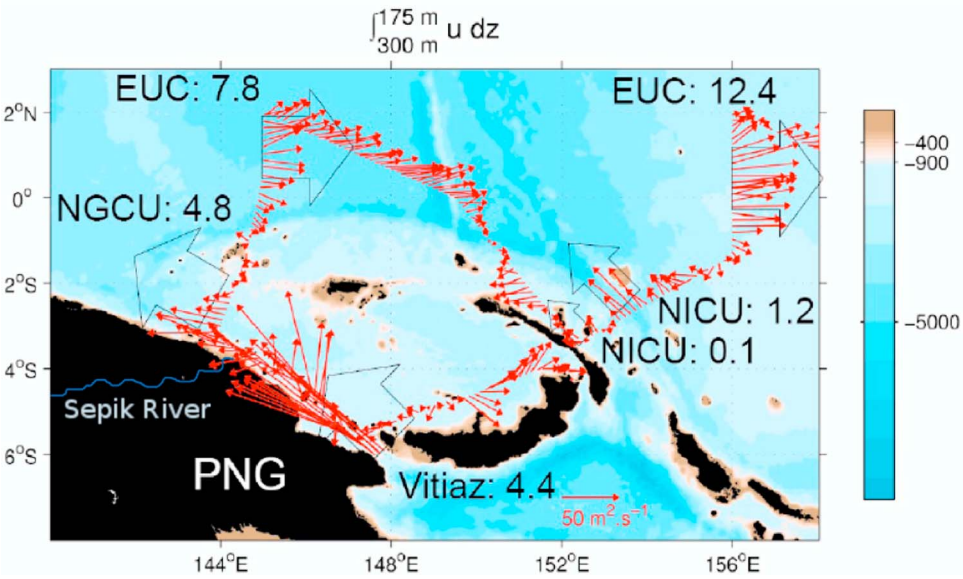

Figure 3. Bathymetric map of Bismarck Sea region overlaid with vectors showing integrated velocity from shipboard ADCP over 175–300 m (corresponding to the depth the EUC). Black box arrows show water volume transport in sverdrups (10^6 m^3s^{-1}).

profiles show (1) high-salinity seawater from the subtropical gyre in the South Pacific entered Vitiaz Strait (station 30) with relatively low total acid-soluble metal concentrations; (2) on the upstream side of the Sepik River (station 29), concentrations of all trace metals were elevated relative to values in Vitiaz Strait at most depths throughout the water column, and at all depths for DMn, TDFe, and TDAl; and (3) total acid-soluble concentrations of all three metals were enriched in surface waters downstream of the Sepik and nearby Ramu Rivers (station 28). The concentrations of both dissolved and total acid-soluble Fe and Mn increased dramatically at 500 m (σ_θ = 26.94 kg m^{-3}) downstream from the Sepik River (from station 29 to station 28). Transmissometry profiles indicated multiple layers of turbid waters, suggesting direct injection of sediment on the upper slope via intermediate nepheloid layers (Figure 5). The greatest local sediment delivery rates have been previously observed along the ~500 m isobath northwest of the Sepik River mouth [*Kuehl et al.*, 2004].

3.3. Zonal Distribution of Trace Metals Along the Equator

[17] Zonal sections along the equator (from 0 to 1000 m) of total acid-soluble Al, Fe, and Mn (TDAl, TDFe, and TDMn,

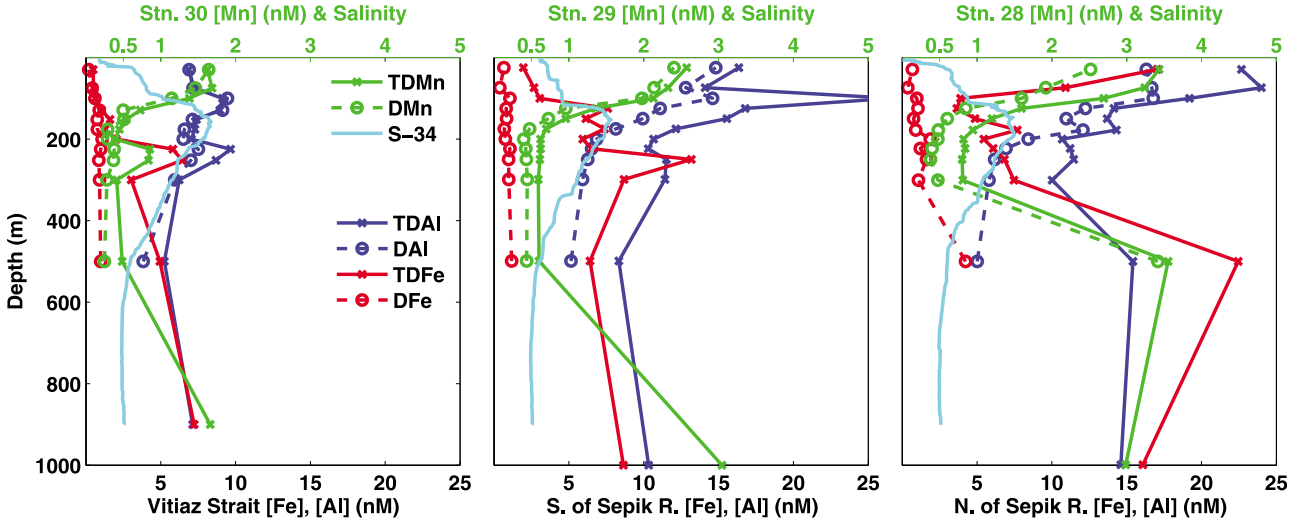

Figure 4. Total acid-soluble and dissolved (<0.4 μm) metal concentrations and salinity for stations 28, 29, and 30 along the northeast coast of Papua New Guinea. Salinity, offset by 34, is shown as a proxy for the depth of the NGCU. Note that Mn has a different scale than Al and Fe.

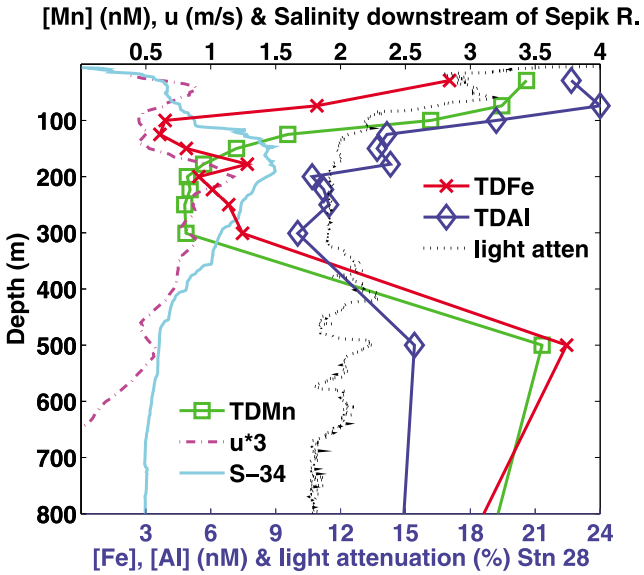

Figure 5. Total acid-soluble metals, alongshore velocity, salinity, and light attenuation (×100) at station 28 with expanded scale bars for TDFe, TDAl, and light attenuation on the bottom axis. Alongshore velocity is resolved to 315° to be parallel to the isobaths offshore the Sepik River. Transmissometry data were recorded from a different cast than the trace metal sampling cast during the same station occupation.

respectively) overlaid with contours of zonal current are shown in Figure 6. The main features are (1) subsurface maxima in total acid-soluble Fe, Mn, and Al within the EUC; (2) the highest trace metal concentrations are in the west near the origin of the EUC and decrease from west to east in the direction of EUC flow; and (3) surface maxima for Al and Mn, but not Fe, in the western Pacific.

[18] An examination of individual station profiles provides detail on the vertical structure and partitioning of the three metals. Profiles of dissolved and total acid-soluble concentrations as well as zonal current are shown at 145°E, 165°E, 170°W, and 155°W in Figure 7 (note the lower concentration scales than Figure 4). The profiles of Fe and Al are compared in the upper figures and Fe and Mn are plotted in the lower figures. We used this approach to enable better visualization of all the data. These profiles exhibited several major features: (1) the subsurface maximum in TDFe along the equator decreased from west to east; (2) DFe displayed nutrient-like profiles with small local maxima coincident with or deeper than the maximum of TDFe at all stations west of 162°E; (3) the subsurface maximum in TDAl was primarily dissolved and occurred up to 75 m shallower in the water column than TDFe; (4) TDAl concentrations decreased continuously from west to east and, of these three metals, correlated most strongly with the core velocity of the EUC; and (5) the subsurface maximum of TDMn was, like Fe, not associated with a large dissolved maximum and was ~20–80 m deeper than the EUC velocity maximum. In contrast, the vertical profiles of DMn displayed a scavenged-like profile along the equator (surface enrichment and depletion at depth).

[19] The depth of subsurface TDAl maxima had a strong (r = 0.88) and significant (P < 0.05) correlation with the depth of the maximum zonal current along the equator: both shoaled from west to east. Along the isopycnal surfaces corresponding to the upper and lower EUC, the total acid-soluble metal concentrations of all three metals decreased eastward significantly (Figure 8). Average TDFe concentrations were always greatest in the lower EUC while average TDAl concentrations were either greatest in the upper EUC or the same within analytical uncertainty (1% difference). Average TDMn concentrations were greatest in the lower EUC west of 170°W. East of 170°W a subsurface TDMn maximum was no longer detectable.

[20] Our concentrations of TDFe and DFe at 155°W agree well with those of *Measures et al.* [2006]. The research group of Measures has found variable surface Fe concentrations at the equator and 140°W on three occasions. On one of their transects, surface Fe concentrations were low (0.05 n*M*) and comparable to those of *Gordon et al.* [1997]. The other two times surface dissolved Fe was higher (~0.2–0.3 n*M*) [*Yang et al.*, 2009; *Hiscock et al.*, 2008]. One of those cruises included an equatorial section from 140°W to the east [*Kaupp et al.*, in press], at which time the low surface Fe concentrations were displaced to the east. Thus, it appears that DFe can be variable at 140°W depending on the east-west displacement of the pool of low Fe surface water. The absence of very low Fe concentrations was corroborated by observations of elevated nitrogen fixation rates near the dateline during this survey [*Bonnet et al.*, 2009].

3.4. Western Pacific Warm Pool Surface Enrichment

[21] Surface concentrations of total acid-soluble Al and Mn were greatest downstream from the Sepik River at station 28 and elevated throughout the western Pacific warm pool. Surface Al and Mn concentrations decreased to baseline levels at the salinity front at 180°W (average of 2.7 and 0.63 n*M* east of the dateline for Al and Mn, respectively, Figures 2 and 6). This front delineates the eastern boundary of the warmer, fresher waters composing the equatorial warm pool. The oceanic response to intermittent westerly wind bursts prior to and during our sampling was apparent in Ocean Surface Current Analyses sea surface velocity fields. The front likely limited any wind-associated eastward advection of elevated surface Mn and Al concentrations beyond the warm pool. DMn values on the equator were as high as 2.5 nM at 145°E, similar to the range of surface values reported by *Mackey et al.* [2002a], and decreased eastward through the warm pool to 1.06 n*M* by 180°W. Likewise, DAl concentrations in the surface water decreased eastward from the Papua New Guinea platform to the dateline. East of the warm pool, both DMn and DAl concentrations were uniformly lower (average ~3 n*M* for DAl, ~0.7 n*M* for DMn) than in the warm pool.

[22] Aeolian supply is considered to be the main source of trace metals to open ocean surface seawater [e.g., *Klinkhammer and Bender*, 1980; *Orians and Bruland*, 1986]. The composition and concentration of atmospheric aerosols were measured during our cruise by *Shank and Johansen* [2008] and were within the range of previous model studies and data-model comparisons, showing extremely low equa-

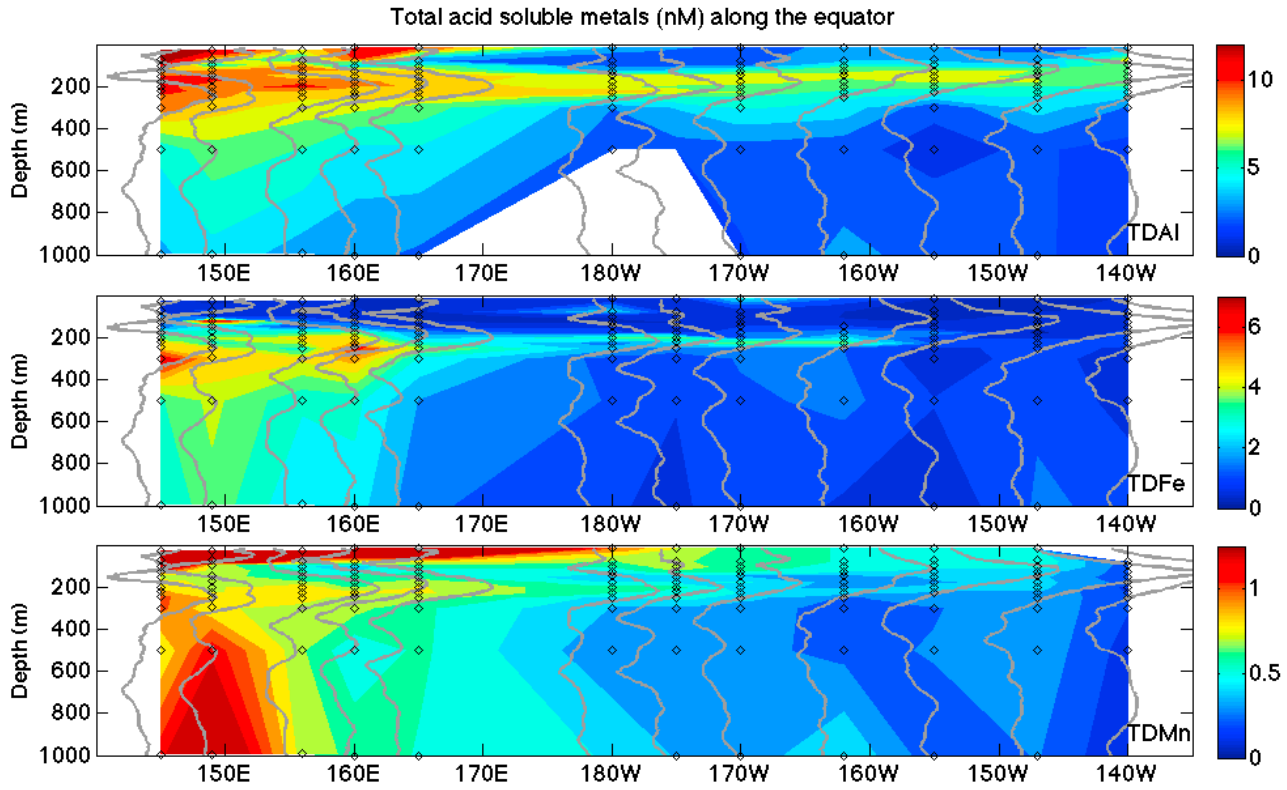

Figure 6. Total acid-soluble aluminum, iron, and manganese along the equator from 145°E to 140°W. The maximum color scale for Al and Mn was set at 12 and 1.25 nM, respectively, to allow the resolution of vertical features. Sample points are indicated by black diamonds. TDAl samples at 175°W were not included because measured TDAl concentrations were lower than the DAl measurements at this station. Zonal current for each station is overlain as gray profiles.

torial deposition and slightly elevated deposition in the Bismarck Sea [*Duce and Tindale*, 1991; *Ginoux et al.*, 2001; *Mahowald et al.*, 2005]. The measurements by *Shank and Johansen* [2008] included aerosol Al, Ti, Mn, and Fe in multiple size classes measured by inductively coupled plasma-mass spectrometry following a 3 day, three acid digestion [*Johansen and Hoffmann*, 2003]. This more extensive acid digestion likely yielded a greater detectable portion of matrix-bound metals than our 24 h pH 1.8 acidification, and thus serves as an upper limit estimate of the magnitude of the atmospheric source. Direct Al measurements were probably contaminated from the aluminum aerosol collector, so Al concentrations were derived from measured Ti by assuming a constant crustal Al/Ti ratio. *Shank and Johansen* [2008] calculated atmospheric fluxes by assuming a depositional velocity for each of three size classes.

[23] To evaluate the possibility that the western warm pool surface maxima for Mn and Al arose from atmospheric deposition, we used atmospheric flux averages from two regions along our cruise track (Figure 1). A lower-bound estimate was determined using atmospheric fluxes to the warm pool (area encompassing stations 13–23 and 25–27). An upper-bound estimate was obtained using fluxes to the Bismarck Sea region (area encompassing stations 24 and 28–30). We calculated the inventory of Mn and Al in the surface waters of the warm pool by integrating from the surface to the maximum depth of the elevated surface metal concentrations on a station-by-station basis. The depth of elevated surface TDAl concentrations (15–100 m, average 52 m) was shallower than the mixed layer depth (50–90 m, average 73 m, based on examination of density and temperature data), except at 145°E. The depth of elevated surface TDMn concentrations (75–145 m, average 108 m) extended below the mixed layer depth, but because the depth of the mixed layer was variable, we chose to consider the entire inventory of surface-enriched water. The average warm pool surface-enriched inventories are reported in Table 1. To calculate the residence times of surface layer TDMn and TDAl, we used both the low (warm pool) and high (Bismarck Sea) estimates of atmospheric fluxes (Table 1).

[24] When using the lower warm pool atmospheric fluxes, the residence times for Mn and Al in the warm pool were 64 years and 15 years, respectively. These are several times larger than typical estimates of Mn and Al residence times in the surface oceans: 5–25 years for Mn [*Klinkhammer and Bender*, 1980] and 3–4 years for Al [*Orians and Bruland*, 1986]. This approach using western warm pool fluxes suggests that atmospheric deposition is not sufficient to explain the surface maxima. Other sources would be required.

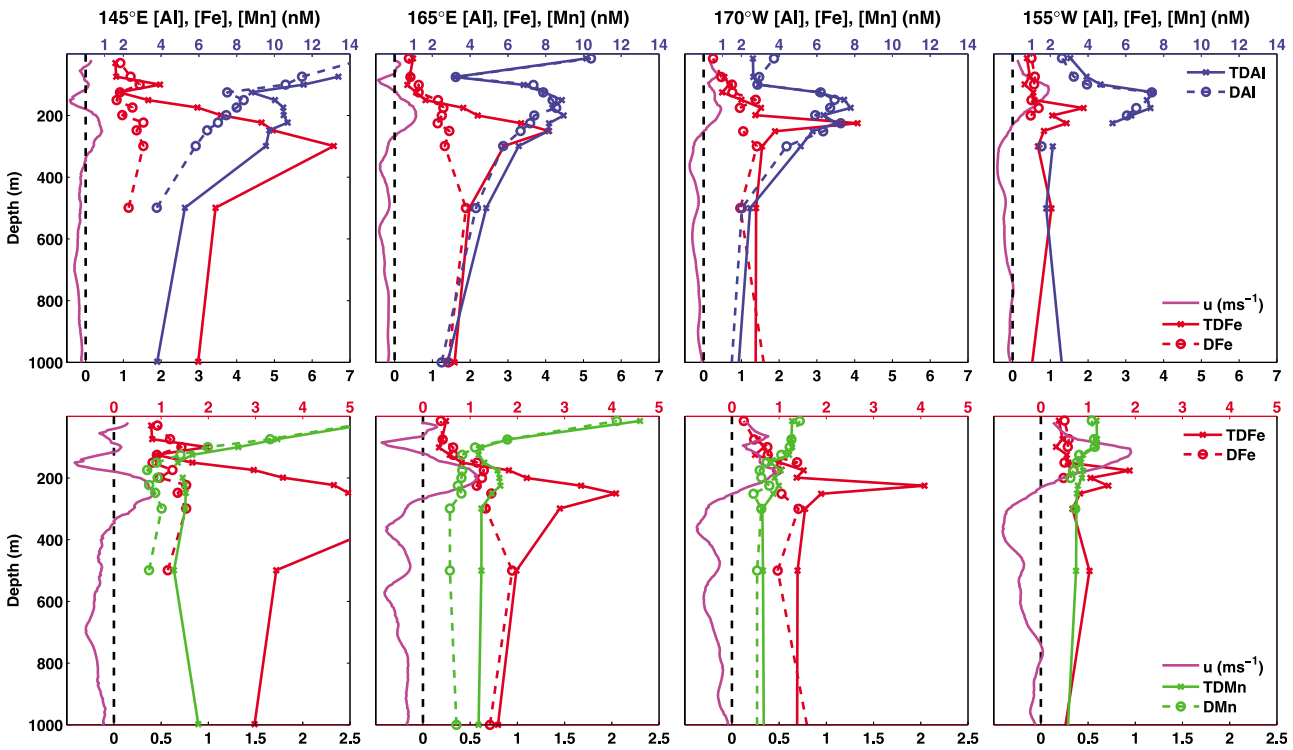

Figure 7. Metals as in Figure 4 for selected equatorial stations. (top) Al (upper blue axis) and (bottom) and Mn (lower black axis). Fe and zonal current included in all frames (axis nearest legend key). Zonal current is shown as a solid pink line. Zero value is indicated by a dashed black line.

[25] In contrast, the atmospheric fluxes measured in the Bismarck Sea were significantly higher and thus the estimated residence times were lower: 5 years and 50 days for Mn and Al, respectively. The larger aerosol fluxes to the Bismarck Sea reflect the atmospheric trajectories of the air masses, which crossed over local islands. If similar atmospheric deposition fluxes occurred in the warm pool or if a significant fraction of the Bismarck Sea–deposited metals were advected to the warm pool, estimated Mn and Al residence times would be much shorter and consistent with, or less than, literature values (Table 1). Atmospheric trajectories and surface currents in the warm pool are variable, thus atmospheric deposition cannot be ruled out as an explanation of the high surface concentrations of Al and Mn in the warm pool.

[26] Surface DFe concentrations along the Papua New Guinea coast and at 145°E were also elevated, but over a shorter length scale than Al and Mn, probably due to the biological uptake of Fe. DFe in surface water was 0.19 n*M* in Vitiaz Strait (station 30), increased to 0.68 n*M* along the Papua New Guinea coast (station 28) and increased further to 0.79 n*M* at 0.6°N, 145°E (station 26). DFe concentrations were high (slightly less than 1.5 μmol/kg) in the Sepik River [*Sholkovitz et al.*, 1999], but such high concentrations were not observed in the surface waters of the Bismarck Sea because Fe is removed more rapidly than Mn or Al by several estuarine processes. DFe concentrations along the Papua New Guinea coast are of similar magnitude to those measured in other ocean margin data sets. For example, in the Bay of Biscay, surface DFe varied from 0.73 n*M* to 0.40 n*M* [*Laës et al.*, 2007]. Surface DFe decreased from >1.4 n*M* to 0.15 n*M* along a transect from central California to Hawaii [*Johnson et al.*, 2003; *Elrod et al.*, 2004]. Similar values were found in coastal Oregon waters by *Chase et al.* [2002]. Surface values were of the same magnitude in the Philippine Sea (0.25 n*M*) and Sulu Sea (0.75–1.48 n*M*) [*Kondo et al.*, 2007]. In the eastern North Pacific HNLC region, *Johnson et al.* [2005] observed elevated surface DFe values of 1.2 nM in an emergent eddy.

[27] Since no surface maximum was evident in Fe at any of the equatorial stations and surface Fe did not show a notable zonal gradient, we used a different approach to evaluate the contribution of atmospheric fluxes. In addition to the total acid-soluble Fe aerosol measurements described above, *Shank and Johansen* [2008] determined atmospheric concentrations of "labile" Fe by brief (5 min) acidification to pH <1.8 and addition of hydroxylamine to reduce Fe (III) to Fe (II). This is a shorter acidification than we used for our seawater samples. The operationally defined measurements of reactive Fe in aerosols and seawater are not directly comparable but still enable us to make a qualitative assessment of the role of an atmospheric source. We calculated the expected concentration of Fe in the equatorial surface mixed layer using average labile Fe (18 nmol m^{-2} d^{-1}) and total Fe (186 nmol m^{-2} d^{-1}) deposition fluxes determined by *Shank and Johansen* [2008] for the entire equatorial region

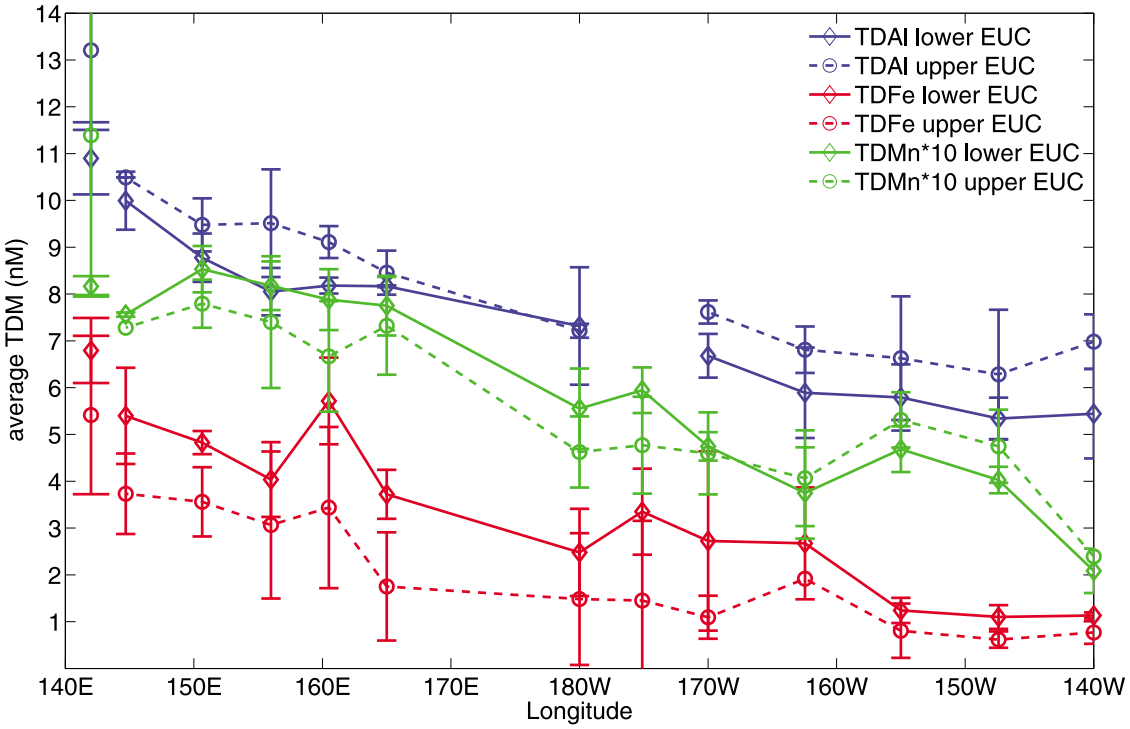

Figure 8. Average TDAl (blue), TDFe (red), and TDMn (green) concentrations along the upper (σ_θ = 23.0–25.8 kg m^{-3}, circles, dashed line) and lower (σ_θ = 25.8–26.6 kg m^{-3}, diamonds, solid line) EUC. Average total acid-soluble metal concentrations for the same isopycnal range at station 28, offshore of Papua New Guinea, are included on the left side of the figure. Error bars are one standard deviation of all measurements within that EUC layer and exceed the analytical error.

(stations 1–27, excluding station 24), an average mixed layer depth along the equator (59 m), and a Fe residence time of 150 days based on reported surface water Fe residence times (~130 days by *Boyle et al.* [2005] and 100 days by *Frew et al.* [2006]). The average equatorial mixed layer depth was calculated from a 0.2°C departure from sea surface temperature. The projected concentration from labile Fe fluxes was 0.05 n*M*; from total Fe fluxes it was 0.48 n*M*. The average concentration of TDFe, for which we have better spatial coverage than DFe, for all equatorial stations, excluding an anomalously high value at 170°W, was 0.52 n*M*. Thus, atmospheric fluxes of labile Fe alone are not enough to explain this value. Total Fe deposition may be solubilized by photochemistry and biological cycling [*Johnson et al.*, 1994; *Sunda and Huntsman*, 1995; *Barbeau and Moffet*, 2000; *Kuma et al.*, 2000] or there may be another source (such as from local rivers). Average atmospheric fluxes of labile Fe to the Bismarck Sea region were only 50% greater than labile Fe fluxes to the equatorial region, so the inclusion of a western atmospheric source does not significantly change this estimate. However, the average magnitude of total aerosol Fe fluxes in the Bismarck Sea were an order of magnitude greater than equatorial total aerosol Fe fluxes, so if only a fraction of this aerosol source were solubilized and advected, it could be a significant source of surface Fe.

3.5. Sedimentary Flux in Western Source Region

[28] Detrial sediment input directly from rivers and diagenetic remobilization are plausible supply mechanisms of trace metals to the NGCU, and we investigate their contributions. The NGCU flows northwest through Vitiaz Strait along the Papua New Guinea slope and outer shelf, which is <10 km at its widest [*Fine et al.*, 1994; *Kineke et al.*, 2000; *Creswell*, 2000]. To estimate a per-area sediment-water flux of metals from New Guinea margin sediments to the NGCU, we divided our estimated net metal flux by the area of sediment-

Table 1. Atmospheric Depositional Fluxes of Manganese and Aluminum in the Western Warm Pool and Bismarck Sea and Estimated Mixed Layer Residence Times

	Average Inventory of Surface Enrichment (nmol m^{-2})	Atmospheric Flux to Warm Pool (nmol m^{-2} d^{-1})	Estimated Residence Time From Warm Pool Fluxes	Atmospheric Flux to Bismarck Sea (nmol m^{-2} d^{-1})	Estimated Residence Time From Bismarck Sea Fluxes	Literature Residence Time (Years)
Al	5.4 × 10^5	98	15 years	10,788	50 days	3–4 [*Orians and Bruland*, 1986]
Mn	1.5 × 10^5	6.3	64 years	78	5.2 years	5–25 [*Klinkhammer and Bender*, 1980]

Table 2. Sediment Flux of Dissolved and Total Acid-Soluble Iron and Manganese From the New Guinea Shelf and Slope and Worldwide Diffusive Flux Estimates

Region	Fe (μmol m^{-2} d^{-1})	Mn (μmol m^{-2} d^{-1})	Reference
Apparent sediment flux of dissolved metals across upper slope (175–300 m)	80	24	This study
Apparent sediment flux of total acid-soluble metals across upper slope (175–300 m)	535	49	This study
Gulf of Papua inner shelf (40–55 m)	−41 to 310	23–112	*Alongi et al.* [1996]
California shelf	−0.2 to 18		*Elrod et al.* [2004]
Oregon-California shelf	<10 to >~300		*Severmann et al.* [2010]
Biogeochemical model with simplified sediment source	2 for depth <1100 m		*Moore et al.* [2004]
California margin, oxygen minimum zone		0–8	*Johnson et al.* [1992]
Eastern Pacific oxygen minimum zone		4.3–20	*Nameroff* [1996]
Extrapolation from organic carbon oxidation from Sepik River using Fe/C from California margin	2.3		*Burns et al.* [2008]; *Elrod et al.* [2004]

water interface on the slope in contact with the same depth interval. Net trace metal fluxes from the upper slope were calculated as the difference between the metal fluxes (175:300 m depth-averaged [TDFe], [DFe], [TDMn], or [DMn] × 175:300 m integrated water volume transport) through the Vitiaz Strait (station 30) and our northern NGCU station at 143°E (station 28). Water volume transports within the 175:300 m depth range, corresponding with the pycnocline (σ_θ = 24.55:26.6 kg m^{-3}), across the NGCU and Vitiaz Strait were calculated from ADCP data from cross-slope and cross-strait transects along our cruise track (Figure 3). Transport through Vitiaz Strait was 4.4 Sv and increased to 4.8 Sv at 143°E. These single transects do not capture the sizable variability in NGCU flow [*Ueki et al.*, 2003] but represent the magnitude of water volume transport during our sampling. We assumed that the width of the slope between the 175 and 300 m isobars was ~5 km, an upper-bound estimate of the ~1 km slope between these isobars [*Kineke et al.*, 2000; *Kuehl et al.*, 2004]. Thus, these per-area flux estimates must be considered lower estimates because they overestimate the area of the sediment-water interface.

[29] These flux estimates for DFe and DMn are large compared with diffusive sediment fluxes reported at most other locations (Table 2). The exceptions are very large diffusive bottom lander flux measurements from continental shelves with large riverine detrital input [*Severmann et al.*, 2010]. However, the Papua New Guinea margin is different as it has essentially no shelf, and most of the sediment from rivers (85–93% for the Sepik River) is channelled rapidly down submarine canyons to deeper sites of deposition [*Kineke et al.*, 2000; *Kuehl et al.*, 2004]. We also estimated the DFe flux from the NE coast of New Guinea using remineralization rates of organic carbon [*Burns et al.*, 2008] (Table 2). We converted the carbon oxidation rate to a DFe flux using the Fe/C flux ratio determined by *Elrod et al.* [2004] off the California coast and the deposition area and organic carbon oxidation rates based on inputs from the Sepik River reported by *Burns et al.* [2008]. Fe reduction coupled to oxidation of organic carbon can potentially be driven by organic matter originating from many rivers besides the Sepik, such as the smaller Ramu River. Nevertheless, much of riverine organic material from northeastern Papua New Guinea is deposited downslope and in slope canyons deeper than the NGCU [*Kineke et al.*, 2000] and may not be relevant.

[30] The large apparent fluxes from the upper slope support the importance of trace metal fluxes from reactive ocean margins and implicate sediment discharge as the most important contribution to these fluxes. Previous studies of coastal and open ocean Fe exchange highlighted the influence of shelf width on dissolved Fe flux [*Bruland et al.*, 2005; *Chase et al.*, 2007; *Cullen et al.*, 2009]. These studies documented that dissolved Fe concentrations over wider shelves were higher than dissolved Fe over narrower continental shelves at numerous sites along the east Pacific margin from Peru to British Columbia. *Cullen et al.* [2009] proposed that wider shelves allow longer sediment-water interaction time and result in elevated concentrations due to diffusive fluxes from reducing sediments. Papua New Guinea and New Ireland have some of the narrowest shelves of any continental margin. The large particulate Fe flux relative to dissolved Fe flux we observed suggests erosional input of particulate metals in the high-energy LLWBCs can play an important role in margin fluxes as well.

[31] Sediment injection via nepheloid layers is supported by the existence of layers of high total suspended matter present offshore from the Papua New Guinea coast [*Mackey et al.*, 2002a; 2002b]. Downstream of the Sepik River (station 28), we observed maxima in light attenuation measured from a separate CTD cast that corresponded to maxima in total metal concentrations (Figure 5). The largest concentrations of trace metals at station 28 were observed at 500 m. Water at this depth is at too great a density to contribute to the EUC. Nevertheless, metal concentrations at station 28 and 29 were elevated throughout the depth range of the NGCU relative to "background" concentrations at Vitiaz Strait (station 30). Friction of strong alongshore currents along the sediment-water interface may also inject particles offshore via Ekman transport [e.g., *Cullen et al.*, 2009].

[32] Although detrital sediment input appeared to play a major role in the increase of trace metal transport in the NGCU along the Papua New Guinea margin, the greater relative increase in DMn and DFe relative to DAl flux (50% and 58%, versus 10%, respectively) from station 30 to 28 suggests the release of reduced Fe and Mn from the sediments

may also be important. Mn and Fe are redox-sensitive metals while Al is not. Mn and Fe have similar but distinct redox behavior. TDFe flux nearly doubled from station 30 to 28 (97% increase), which could be explained by rapid redox cycling [e.g., *Canfield et al.*, 1993] as well as mechanical dispersal. The surface sediments of the continental slope are well oxygenated as indicated by their rusty orange color [*G.J. Brunskill*, unpublished data, 1996]. *Pakhomova et al.* [2007] found that sediment resuspension, bioirrigation, and chemical processes at the interface are much more important for Fe fluxes than for Mn fluxes in multiple study regions. They concluded that Mn flux depended less on bottom water oxygen concentrations than Fe flux. Instead, Mn flux strongly depends on the concentration of Mn in pore water. Physical processes can result in Fe fluxes up to an order of magnitude greater than diffusion alone. On the basis of the magnitude of our lower-bound per-area dissolved and total acid-soluble metal fluxes, sedimentary diagenetic remobilization alone appears unlikely to be the main metal flux. We do not presently have sufficient data to quantify the relative magnitude of redox-driven and physical fluxes in this region of high sediment discharge and strong tidal and western boundary currents.

[33] Recent work in the western subarctic Pacific demonstrates that both redox-driven and mechanical mobilization from continental margins can be important sources of particulate Fe. *Lam and Bishop* [2008] observed a persistent (weeks) ~50 m separation between the subsurface maxima of particulate Fe (deeper) and Mn (shallower). The maximum in particulate Mn in the subarctic Pacific occurred on the same density surface as anoxic shelf sediments where redox-driven remobilization of both Mn (II) and Fe (II) and subsequent oxidation and precipitation could supply currents with Mn and Fe. They attributed the deeper maximum in particulate Fe maximum to additional episodic resuspension of sedimentary material from the basaltic slope. We observed a similar pattern of a persistent (basin-scale) vertical separation in subsurface metal maxima. The deeper TDFe and TDMn maxima and shallower DAl maxima in the equatorial Pacific may reflect differences in a depth-dependent source of these metals.

3.6. Distribution and Transport of Trace Elements in the EUC

[34] As described in section 3.3, the depths and zonal extents of maxima associated with the EUC were different for Al, Mn, and Fe (Figure 7). The TDAl maximum was shallower than those for TDMn and TDFe. The TDMn maximum did not extend as far east as the TDAl and TDFe maxima. These features are presented on EUC density surfaces in Figure 8, which shows the average equatorial metal concentrations in the upper (σ_θ = 23.0–25.8 kg m^{-3}) and lower (σ_θ = 25.8–26.6 kg m^{-3}) EUC. The differences between the distribution of TDAl, TDMn, and TDFe suggest they have different sources and/or sinks. Possible sources include local processes such as atmospheric deposition and remineralization and advection. Possible sinks include scavenging and dilution (advection under a different guise). We will examine each of these sources and sinks in turn.

3.6.1. Local Processes

[35] In their model of aluminum for dust calculation in oceanic waters hypothesis, *Measures et al.* [2008b] suggested that elevated surface Al concentrations may indicate a dust-derived source of Fe to the euphotic zone. *Measures et al.* [2008b] proposed that the subsurface maximum in dissolved Fe observed in the subtropical Atlantic resulted from a surface-deposited dust source followed by biological uptake, vertical export, and remineralization in the oxygen minimum zone. The EUC is not associated with an oxygen minimum zone but does accumulate regenerated nutrients [e.g., *Toggweiler and Carson*, 1995]. We estimated the potential contribution of an aerosol iron source that is fully exported and remineralized in the EUC. We used the aerosol data of total Fe aerosol from *Shank and Johansen* [2008] (section 3.4) to constrain the flux of Fe. We assumed the total Fe flux was entirely remineralized within the EUC density range (σ_θ = 23.0–26.6 kg m^{-3}) and had a 150 day residence time. This aerosol Fe source could contribute between 0.19 and 0.38 n*M* of Fe, depending on the thickness of the EUC. This range is much lower than observed concentrations of DFe (0.57–1.4 n*M*) and TDFe (0.77–4.5 n*M*) in the EUC. Thus, another source is required to supply the Fe in the EUC.

[36] As discussed in section 3.4, upper-bound estimates atmospheric fluxes of Al and Mn are required to explain the surface enrichment of Al and Mn in the western equatorial Pacific, so it appears unlikely that atmospheric deposition could also supply the subsurface maxima in Al and Mn.

3.6.2. Scavenging

[37] Water column profiles show that Al, Mn, and Fe are actively scavenged onto sinking particles [e.g., *Klinkhammer and Bender*, 1980; *Orians and Bruland*, 1986; *Johnson et al.*, 1997]. Estimates of particulate Fe residence times in the mixed layer are on the order of 150 days [*Boyle et al.*, 2005; *Frew et al.*, 2006]. The residence time of Fe below the euphotic zone is likely to be longer than this mixed-layer estimate because particle concentrations are lower. The average velocity of the EUC from 180°W to 140°W along the equator was 41 cm s^{-1}. This yields a transport time estimate of 124 days, neglecting recirculation. Scavenging is likely to contribute to Fe loss on such timescales. However, comparing the west–to–east zonal gradient in TDFe concentrations with those of TDMn and TDAl suggests that scavenging is not the dominant loss mechanism. Mn typically has a slower scavenging loss rate than Fe and Al [*Landing and Bruland*, 1987]. The zonal gradient in TDMn concentrations in the EUC was similar to than those of TDFe and TDAl (Figure 8). Scavenging of Fe might have contributed to the vertical separation between the TDAl maxima and TDFe maxima. However, if preferential scavenging of DFe in the upper EUC was the cause of the observed separation, it is difficult to imagine a mechanism that would concentrate sinking scavenged Fe at the base of the EUC. In addition, the offset between the TDFe and TDAl is relatively constant and a differential scavenging mechanism should result in increasing separation downstream.

3.6.3. Advection and Dilution

[38] Both previous work [e.g., *Gordon et al.*, 1997; *Lacan and Jeandel*, 2001] and the zonal gradient in trace element concentrations and the relative magnitude of surface sources

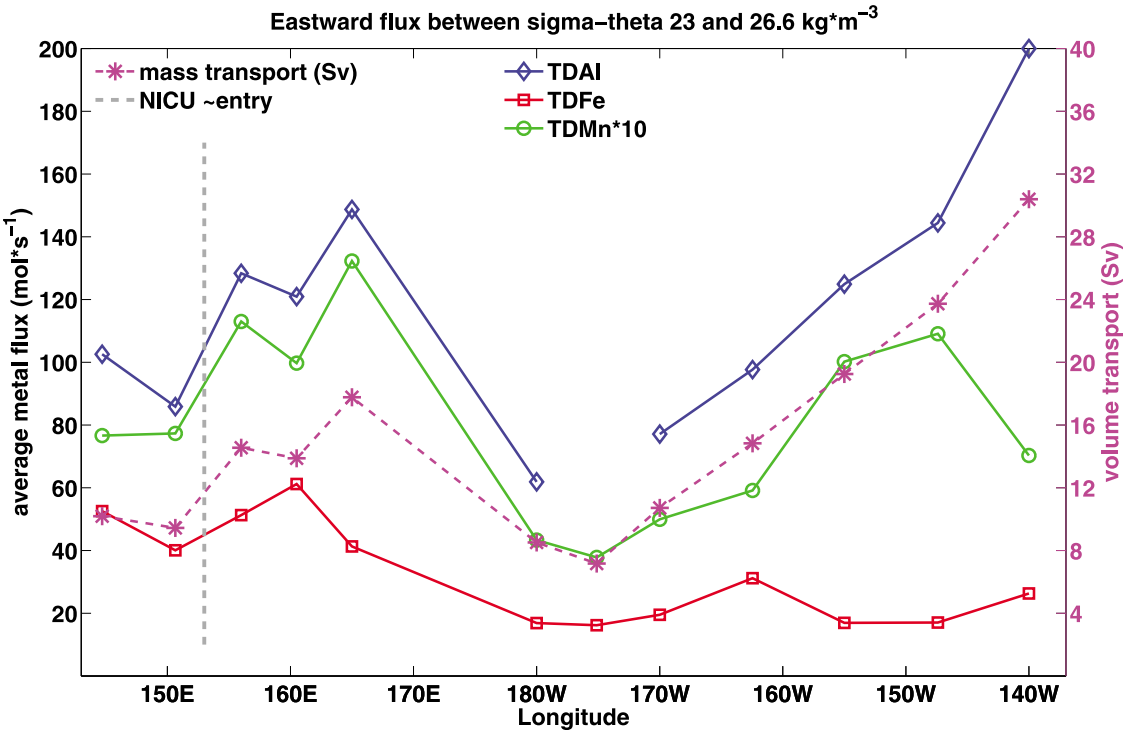

Figure 9. Eastward flux of TDAl (blue diamonds), TDFe (red squares), and TDMn (green circles), and volume transport (pink asterisks) along the equator between $\sigma_\theta = 23.0$ and 26.6 kg m^{-3}. See text for explanation of calculation. Dashed gray line indicates approximate entry longitude of the NICU into the EUC.

reported here suggest that the EUC is responsible for transporting lithogenic material to the eastern equatorial Pacific. However, the extent of coastal sources of trace elements to the open ocean is presently poorly constrained [*Henderson et al.*, 2007]. We used our shipboard ADCP data and trace element concentrations to estimate the magnitude and pattern of eastward transport of TDAl, TDMn, and TDFe within the EUC. We integrated instantaneous water volume fluxes along the upper and lower EUC (eastward flow between $\sigma_\theta = 23.0$–25.8 kg m^{-3} and $\sigma_\theta = 25.8$–26.6 kg m^{-3}, respectively) within 2° of the equator from shipboard ADCP data and multiplied volume transport by the average equatorial metal concentrations in the upper and lower EUC (Figure 8). The flux of TD metal M at each longitude is calculated as

$$\int_{23.0}^{26.6} \text{TDM flux (EUC)} = \int_{23.0}^{25.8} (u\ \mathrm{d}\ z)\ \overline{\text{TDM}}\ \text{(upper EUC)} + \int_{25.8}^{26.6} (u\ \mathrm{d}\ z)\ \overline{\text{TDM}}\ \text{(lower EUC)},$$

where u is the integral of eastward current 2°S–2°N and z is depth of the designated potential density at the equator. Fluxes of TDAl, TDFe, and TDMn and EUC water volume are shown in Figure 9.

[39] Uncertainties in the flux estimates exist due to the differing time and space scales of integration of the velocities and metal concentrations. ADCP data were collected as the cruise was underway, and metal concentrations at a particular station are a cumulative record of earlier transports. Care must also be taken in interpreting the magnitude of metal transports because our calculations applied metal concentrations measured at the equator to the entire 4° meridional breadth of the cruise track. However, subdividing our flux integration into three meridional bins at longitudes for which TDAl and TDMn measurements were available at 2°N and 2°S did not change the zonal trend in metal transport (not shown).

[40] The patterns of the three trace metal fluxes were similar west of the dateline but diverged east of the dateline. West of the dateline, total metal transport generally increased from 145°E to ~160°E–165°E, downstream of the NICU entry longitude (Figure 9, dashed line [*Butt and Lindstrom*, 1994]). Water volume flux increased similarly and was within the range reported by *Johnson et al.* [2002, Figure 17], especially during El Niños. The entry point for the NGCU is not well understood, so we did not display a longitude for entry of the NGCU in Figure 9. Tracer data suggest the NGCU retroflects across the equator before joining the eastward flowing EUC near its origin [*Tsuchiya et al.*, 1989; *Fine et al.*, 1994]. Inverse modeling suggests the NGCU enters further east, between 156°E and 170°W [*Sloyan et al.*, 2003]. Almost every increase in metal transport was accompanied with an increase in water volume transport, implying the primary sources of trace elements were not local processes. Rather than exhibiting a continuous metal concentration decrease from 145°E eastward (i.e., from continual scavenging losses), trace element concentrations in the western EUC remained

constant within uncertainty bounds (or, as for TDFe in the lower EUC, increased) from 145°E to 160°E (Figure 8). Trace element fluxes at 160°E were greater than those at 145°E and 149°E (Figure 9). The coincident increase in metal transport and water volume transport implies entering southern LLWBCs contributed trace elements to the EUC.

[41] East of the dateline, water volume transport increased, consistent with the entrainment of subtropical water into the EUC. However, TDFe flux remained constant within the uncertainties of our estimate. In contrast, TDAl and TDMn fluxes generally increased coincidently with water volume fluxes. The primary source of increased transport of the EUC in the interior Pacific is thought to be meridional entrainment of Southern Hemisphere subtropical water [*Johnson and McPhaden*, 1999]. Evidently, entering subtropical water has lower Fe concentrations and similar Al and Mn concentrations as the EUC water entering from the west. A comparison of the respective density horizons of the metal maxima yields some insight. Most of the increase in water volume and Al and Mn flux occurred in the upper EUC (100–165 m). Across this depth range, Al concentrations were greatest at the equator relative to 2°N and 2°S (except at the dateline, where the EUC meanders) and Mn concentrations had no distinct meridional trend in the central equatorial Pacific (not shown). Therefore, the entrained subtropical water appears to come from deeper water masses with greater metal concentrations. Such a circulation pattern is consistent with isopycnal flow along the doming equatorial isopycnals. Diapycnal mixing in shallow tropical recirculation cells, driven by air-sea interactions, is known to occur in the upper thermocline layers [*Lu et al.*, 1998].

[42] The highest concentrations and largest fluxes of TDFe occurred in the lower EUC within the lower-velocity but higher-flux 13°C Water. Fluxes at the base of the EUC experience different dynamical controls than those in the upper EUC. Inverse models show less vertical mixing in the lower thermocline than in the upper thermocline (essentially the upper EUC) [*Johnson et al.*, 2002; *Sloyan et al.*, 2003]. Zonal trends in metal concentrations within the EUC were consistent with these dynamics. Average TDAl, TDFe, and TDMn concentrations decreased significantly ($P < 0.001$) eastward along both the upper and lower EUC isopycnal surfaces. The lower EUC had stronger correlations of metal concentration with longitude (correlation coefficients closer to +1) than the upper EUC ($r = -0.93$ versus -0.89, -0.98 versus -0.94, -0.95 versus -0.88 for TDFe, TDAl, and TDMn, respectively). Physical processes likely control the tighter longitudinal correlation in the lower EUC. Model advective tracers suggest that ~30% of the source waters of the Niño-3 region (equatorial surface waters between 150°W and 90°W) originate from southern LLWBCs [*Fukumori et al.*, 2004]. However, more than 90% of 13°C water enters the eastern equatorial region through LLWBCs, and the Southern Hemisphere is the largest contributor [*Qu et al.*, 2009]. Thus, the lower EUC represents a "cleaner line" between the putative source region of the Papua New Guinea slope and the central equatorial Pacific. The 13°C Water upwells east of the Galapagos Islands and off the American coast [*Lukas*, 1986] rather than the equatorial upwelling zone. The persistence of the TDFe maximum within the lower EUC may partially explain why, despite significant iron fluxes, persistent iron-limited conditions are maintained in the equatorial upwelling zone. This depth distinction of an EUC-associated Fe maximum has been neglected in previous estimates of Fe upwelling flux that estimated flux from depths more likely to be in the EUC velocity core (upper EUC) [e.g., *Gordon et al.*, 1997; *Wells et al.*, 1999].

3.7. Implications of a Particulate Iron Source

[43] Our data suggest that the majority of iron entrained by the NGCU consists of acid-soluble particles that are included in our measurements of TDFe. Iron in this form is not readily used by phytoplankton [*Shaked et al.*, 2005] but can become bioavailable through photoreduction [*Johnson et al.*, 1994], phagotrophy [*Barbeau and Moffet*, 2000], dissolution [*Kuma et al.*, 2000], and reduction at phytoplankton cell surfaces [*Sunda and Huntsman*, 1995]. Although our zonal transect along the equator did not extend east of 140°W, a TDFe maximum was present at the base of the EUC at this location, between 175 and 225 m. This suggests that long-range transport of TDFe from Pacific New Guinea continental margins to the central Pacific does occur and that this TDFe maximum persists on density surfaces that reach the euphotic zone in the far eastern equatorial Pacific and South American coast.

[44] Data-constrained model simulations suggest that a similar Fe maximum originating at a depth of ~270 m in the western equatorial Pacific would reach the surface of the eastern equatorial Pacific by ~120°W [*Slemons et al.*, 2009]. The inclusion of a western Fe source based on the measurements of TDFe reported here and by *Mackey et al.* [2002a] improved the model's representation of zonal gradients in surface nutrients and patterns of primary productivity and export but overstimulated primary production in the eastern equatorial Pacific, suggesting that only a fraction of the margin-origin TDFe is bioavailable.

4. Conclusions

[45] The western equatorial Pacific has long been recognized as a critical place for interhemispheric and interbasin water transport [*Tsuchiya et al.*, 1989; *Hirst and Godfrey*, 1993; *Fine et al.*, 1994; *Butt and Lindstrom*, 1994]. The present study shows that the western equatorial Pacific is a primary source of the micronutrient iron to the lower waters of the Pacific Equatorial Undercurrent (EUC). The depth and strength of the EUC controls the biogeochemical conditions of the eastern equatorial Pacific [*Barber et al.*, 1996] where HNLC conditions result from iron limitation and grazing of small phytoplankton [*Martin et al.*, 1991; *Frost and Franzen*, 1992; *Murray et al.*, 1994; *Landry et al.*, 1997].

[46] The data presented here suggest the importance of diagenetic remobilization and detrital sediment input from either direct river input or sediment resuspension as sedimentary sources of iron to the open ocean in EUC via the NGCU yet are only a snapshot of a dynamic region. *Ryan et al.* [2006] have hypothesized that the strengthening and shoaling of the NGCU that occurs during El Niño may intermittently increase inputs of iron to the NGCU and subsequently EUC and thus set the timing of blooms in the

eastern equatorial Pacific. Future climate scenarios suggest the possibility for more persistent El Ninõ-like states in the equatorial Pacific [*Meehl and Washington*, 1996], which might imply greater Fe input to the region. However, an iron-explicit biogeochemical model study suggests that variability in a margin Fe source is dampened during the equatorial transit [*Gorgues et al.*, 2010]. Our observations do not provide information on the temporal variability of trace metal fluxes, but these would be expected to depend in some way on the known seasonal and interannual variability of the NGCU [*Creswell*, 2000; *Ueki et al.*, 2003]. Modulation of NGCU mobilization and subsequent transport of iron might act as a throttle on productivity in the eastern equatorial Pacific.

[47] However, the less heralded result of this new data set indicates that it is at best premature to trace iron from the Papua New Guinea slope to the eastern equatorial Pacific upwelling zone. Elevated trace metal concentrations in the NGCU appear to mix more rapidly out of the central thermocline as interior water masses dilute the upper EUC. Average iron concentrations were consistently greater in the lower EUC than in the upper EUC at every equatorial station along our cruise track. Although diapycnal mixing is thought to bring up deeper EUC waters, 13°C water reaches the surface predominantly off the coast of South America [*Lukas*, 1986; *Qu et al.*, 2009]. A strong detrital sediment source followed by rapid advection and relatively little mixing allow the penetration of a subsurface iron maximum in the lower EUC into the central Pacific, decoupled from local atmospheric deposition. Future estimates of iron upwelling rates in the eastern equatorial Pacific should carefully account for sensitive depth-dependent dynamics that shape the biogeochemistry of this region.

[48] **Acknowledgments.** We thank J. Cullen, K. Orians, and R. Francois for generously lending us the Canadian GEOTRACES sampling system. The officers, crew, and marine techs of the R/V *Kilo Moana* excelled at accommodating and anticipating scientific needs. We are grateful to O. Yigiterhan, F. Lacan, and C. Venchiarutti for tirelessly assisting in sample acquisition. We thank K. Johnson and V. Elrod for their willingness to share expertise on iron sampling and analyses. Conversations with T. Gorgues and C. Menkes greatly aided the probing and presentation of the data. G. Brunskill generously shared his archival knowledge of the Papua New Guinea margin. This research was funded by the National Science Foundation's grant to J.W.M. and J.R. NSF-OCE-0425721 as well as JISAO under National Oceanic and Atmospheric Administration (NOAA) Cooperative Agreement NA17RJ1232. This is NOAA-Pacific Marine Environmental Laboratory publication 3467 and Joint Institute for the Study of the Atmosphere and Ocean (JISAO) 1809.

References

Alongi, D. M., S. G. Boyle, F. Tirendi, and C. Payn (1996), Composition and behavior of trace metals in post-oxic sediments of the Gulf of Papua, Papua New Guinea, *Estuarine, Coastal Shelf Sci.*, *42*, 197–211.

Barbeau, K., and J. W. Moffet (2000), Laboratory and field studies of colloidal iron oxide dissolution as mediated by phagotrophy and photolysis, *Limnol. Oceanogr.*, *45*(4), 827–835.

Barber, R. T., M. P. Sanderson, S. T. Lindley, F. Chai, J. Newton, C. C. Trees, D. G. Foley, and F. P. Chavez (1996), Primary productivity and its regulation in the equatorial Pacific during and following the 1991–1992 El Niño, *Deep-Sea Res. Part II*, *43*(4–6), 933–969.

Bonnet, S., I. C. Biegala, P. Dutrieux, L. O. Slemons, and D. G. Capone (2009), Nitrogen fixation in the western equatorial Pacific: Rates, diazotrophic cyanobacterial size class distribution, and biogeochemical significance, *Global Biogeochem. Cycles*, *23*, GB3012, doi:10.1029/2008GB003439.

Boyle, E. A., B. A. Bergquist, R. A. Kayser, and N. Mahowald (2005), Iron, manganese, and lead at Hawaii Ocean time series station ALOHA: Temporal variability and an intermediate water hydrothermal plume, *Geochim. Cosmochim. Acta*, *69*(4), 933–952.

Bruland, K. W., E. L. Rue, G. J. Smith, and G. R. Di Tullio (2005), Iron, macronutrients, and diatom blooms in the Peru upwelling regime: Brown and blue waters of Peru, *Mar. Chem.*, *93*, 81–103, doi: 10.1016/j.marchem.2004.06.011.

Burns, K. A., G. Brunskill, D. Brinkman, and I. Zagorskis (2008), Organic carbon and nutrient fluxes to the coastal zone from the Sepik River outflow, *Cont. Shelf Res.*, *28*, 283–301.

Butt, J., and E. Lindstrom (1994), Currents off the east coast of New Ireland, Papua New Guinea, and their relevance to regional undercurrents in the western equatorial Pacific Ocean, *J. Geophys. Res.*, *99*, 12,503–12,514.

Canfield, D. E., B. Thamdrup, and J. W. Hansen (1993), The anaerobic degradation of organic matter in Danish coastal sediments: Iron reduction, manganese reduction, and sulfate reduction, *Geochim. Cosmochim. Acta*, *57*, 3867–3883.

Chase, Z., P. G. Strutton, and B. Hales (2007), Iron links river runoff and shelf width to phytoplankton biomass along the U.S. West Coast, *Geophys. Res. Lett.*, *34*, L05407, doi:10.1029/2006GL028069.

Creswell, G. R. (2000), Coastal currents of northern Papua New Guinea and the Sepik River outflow, *Mar. Freshwater Res.*, *51*, 553–64.

Cullen, J. T., M. Chong, and D. Ianson (2009), British Columbia continental shelf as a source of dissolved iron to the subarctic northeast Pacific Ocean, *Global Biogeochem. Cycles*, *23*, GB4012, doi:10.1029/2008GB003326.

Duce, R. A., and N. W. Tindale (1991), Atmospheric transport of iron and its deposition in the ocean, *Limnol. Oceanogr.*, *36*, 1715–1726.

Dutrieux, P., C. Menkes, J. Vialard, P. Flament, and B. Blanke (2008), Lagrangian study of tropical instability vortices in the Atlantic, *J. Phys. Oceanogr.*, *38*, doi:10.1175/2007JPO3763.1, 400–417.

Elrod, V. A., W. M. Berelson, K. H. Coale, and K. S. Johnson (2004) The flux of iron from continental shelf sediments: A missing source for global budgets, *Geophys. Res. Lett.*, *31*, L12307, doi:10.1029/2004GL020216.

Fine, R., R. Lukas, F. M. Bingham, M. J. Warner, and R. Gammon (1994), The western equatorial Pacific: A water mass crossroads, *J. Geophys. Res.*, *99*, 25,063–25,080.

Frew, R. D., D. A. Hutchins, S. Nodder, S. Sanudo-Wilhemy, A. Tovar-Sanchez, K. Leblanc, C. E. Hare, and P. W. Boyd (2006), Particulate iron dynamics during Fe cycle in subantarctic waters southeast of New Zealand, *Global Biogeochem. Cycles*, *20*, GB1S93, doi:10.1029/2005GB002558.

Frost, B., and N. C. Franzen (1992), Grazing and iron limitation in the control of phytoplankton stock and nutrient concentration: A chemostat analogue of the Pacific equatorial upwelling zone, *Mar. Ecol.: Prog. Ser.*, *83*, 291–303.

Fukumori, I., T. Lee, B. Cheng, and D. Menemnlis (2004), The origin, pathway, and destination of Niño-3 water estimated by a simulated passive tracer and its adjoint, *J. Phys. Oceanogr.*, *34*, 582–604.

Ginoux, P., M. Chin, I. Tegen, J. M. Prospero, B. Holben, O. Dubovik, and S.-H. Lin (2001), Sources and distributions of dust aerosols simulated with the GOCART model, *J. Geophys. Res.*, *106*(D17), 20,255–20,273.

Gordon, R. M., K. H. Coale, and K. S. Johnson (1997), Iron distributions in the equatorial Pacific: Implications for new production, *Limnol. Oceanogr.*, *42*, 419–431.

Gorgues, T., C. Menkes, Y. Dandonneau, S. Alvain, C. Moulin, L. Slemons, and M.-H. Radenac (2010), Revisiting the La Niña 1998 phytoplankton blooms in the equatorial Pacific, *Deep-Sea Res.*, *57*(4), 567–576, doi:10.1016/j.dsr.2009.12.008.

Henderson, G. M., et al. (2007), GEOTRACES: An international study of the global marine biogeochemical cycles of trace elements and their isotopes, *Chem. Erde-Geochem.*, *67*(2), 85–131, doi:/10.1016/j.chemer.2007.02.001.

Hirst, A. C., and J. S. Godfrey (1993), The role of Indonesian throughflow in a global ocean GCM, *J. Phys. Oceanogr.*, *23*(6), 1057–1086.

Hiscock, W. T., C. I. Measures, W. M. Landing, and C. S. Buck (2008), High-resolution dissolved Fe and Al along 150°W in the north Pacific Ocean: Results from the CLIVAR repeat Hydrography Program P16N section, AGU Fall Meeting, Abstract OS21G-01.

Johansen, A. M., and M. R. Hoffmann (2003), Chemical characterization of ambient aerosol collected during the northeast monsoon season over the Arabian Sea: Labile-Fe(II) and other trace metals, *J. Geophys. Res.*, *108*(D14), 4408, doi:10.1029/2002JD003280.

Johnson, G. C. (2001), The Pacific Ocean subtropical cell surface limb, *Geophys. Res. Lett.*, *28*(9), 1771–1774.

Johnson, G. C., and M. McPhaden (1999), Interior pycnocline flow from the subtropical to the Equatorial Pacific Ocean, *J. Phys. Oceanogr.*, *29*, 3073–3089.

Johnson, G. C., B. M. Sloyan, W. S. Kessler, and K. E. McTaggart (2002), Direct measurements of upper ocean currents and water properties across the tropical Pacific during the 1990s, *Prog. Oceanogr.*, *52*, 31–61.

Johnson, K. S., W. M. Berelson, K. H. Coale, T. L. Coley, V. A. Elrod, W. R. Fairey, H. D. Iams, T. E. Kilgore, and J. L. Nowicki (1992), Manganese flux from continental margin sediments in a transect through the oxygen minimum, *Science*, *257*, 1242–1245.

Johnson, K. S., K. H. Coale, and V. A. Elrod (1994), Iron photochemistry in seawater from the equatorial Pacific, *Mar. Chem.*, *46*(4), 319–334.

Johnson, K. S., R. M. Gordon, and K. H. Coale (1997), What controls dissolved iron concentrations in the world ocean?, *Mar. Chem.*, *57*, 137–161.

Johnson, K. S., et al. (2003), Surface ocean-lower atmosphere interactions in the Northeast Pacific Ocean Gyre: Aerosols, iron, and the ecosystem response, *Global Biogeochem. Cycles*, *17*(2), 1063, doi:10.1029/2002GB002004.

Johnson, K. W., L. A. Miller, N. E. Sutherland, and C. S. Wong (2005), Iron transport by mesoscale Haida eddies in the Gulf of Alaska, *Deep-Sea Res. Part II*, *52*, 933–953.

Kaupp, L. J., C. I. Measures, K. E. Selph, and F. T. Mackenzie (2010), The distribution of dissolved Fe and Al in the upper waters of the Eastern Equatorial Pacific, *Deep-Sea Res. Part II*, doi:10.1016/j.dsr2.2010.08.009, in press.

Kineke, G. C., K. J. Woolfe, S. A. Huehl, J. D. Milliman, T. M. Dellapenna, and R. G. Purdon (2000), Sediment export from the Sepik River, Papua New Guinea: Evidence for a divergent sediment plume, *Cont. Shelf Res.*, *20*, 2239–2266.

Klinkhammer, G. P., and M. L. Bender (1980), The distribution of manganese in the Pacific Ocean, *Earth Planet. Sci. Lett.*, *46*, 361–384.

Kondo, Y., S. Takeda, and K. Furuya (2007), Distribution and speciation of dissolved iron in the Sulu Sea and its adjacent waters, *Deep-Sea Res. Part II*, *54*, 60–80.

Kuehl, S. A., G. J. Brunskill, K. Burns, D. Fugate, T. Kniskern, and L. Meneghini (2004), Nature of sediment dispersal off the Sepik River, Papua New Guinea: preliminary sediment budget and implications for margin processes, *Cont. Shelf Res.*, *24*, 2417–2429.

Kuma, K., J. Tanaka, K. Matsunaga, and K. Matsunaga (2000), Effect of hydroxamate ferrisiderophore complex (ferrichrome) on iron uptake and growth of a coastal marine diatom, *Chaetoceros sociale, Limnol. Oceanogr.*, *45*(6), 1235–1244.

Lacan, F., and C. Jeandel (2001) Tracing Papua New Guinea imprint on the central equatorial Pacific Ocean using neodymium isotope compositions and rare earth element patterns, *Earth Planet. Sci. Lett.*, *186*, 497–512.

Laës, A., S. Blain, P. Laan, S. J. Ussher, E. P. Achterberg, P. Trégeur, and H. J. W. de Baar (2007), Sources and transport of dissolved iron and manganese along the continental margin of the Bay of Biscay, *Biogeosciences*, *4*, 181–194.

Lam, P. J., J. K. B. Bishop, C. C. Henning, M. A. Marcus, G. A. Waychunas, and I. Y. Fung (2006) Wintertime phytoplankton bloom in the subarctic Pacific supported by continental margin iron, *Global Biogeochem. Cycles*, *20*, GB1006, doi:10.1029/2005GB002557.

Lam, P. J., and J. K. B. Bishop (2008), The continental margin is a key source of iron to the HNLC North Pacific Ocean, *Geophys. Res. Lett.*, *35*, L07608, doi:10.1029/2008GL033294.

Landing, W. M., and K. W. Bruland (1987), The contrasting biogeochemistry of iron and manganese in the Pacific Ocean, *Geochim. Cosmochim. Acta*, *51*(1), 29–43.

Landry, M. R., et al. (1997), Iron and grazing constraints on primary production in the central equatorial Pacific: An EqPac synthesis, *Limnol. Oceanogr.*, *42*, 405–418.

Le Borgne, R., R. T. Barber, T. Delcroix, H. Y. Inoue, D. J. Mackey, and M. Rodier (2002), Pacific warm pool and divergence: temporal and zonal variations on the equator and their effects on the biological pump, *Deep-Sea Res. Part II*, *49*, 2471–2512.

Lu, P., J. P. McCreary, and B. A. Klinger (1998), Meridional circulation cells and the source waters of the Pacific Equatorial Undercurrent, *J. Phys. Oceanogr.*, *28*, 62–84.

Lukas, R. (1986), The termination of the equatorial undercurrent in the eastern Pacific, *Prog. Oceanogr.*, *16*, 63–90.

Mackey, D. J., J. E. O'Sullivan, and R. J. Watson (2002a), Iron in the western Pacific: A riverine or hydrothermal source for iron in the Equatorial Undercurrent, *Deep-Sea Res. Part I*, *49*, 877–893.

Mackey, D. J., J. E. O'Sullivan, R. J. Watson, and D. Dal Pont (2002b), Trace metals in the western Pacific: Temporal and spatial variability in the concentrations of Cd, Cu, Mn, and Ni, *Deep-Sea Res.*, *49*, 2241–2259.

Mahowald, N. M., A. R. Baker, G. Bergametti, N. Brooks, R. A. Duce, T. D. Jickells, N. Kubilay, J. M. Prospero, and I. Tegen (2005), Atmospheric global dust cycle and iron inputs to the ocean, *Global Biogeochem. Cycles*, *19*, GB4025, doi:10.1029/2004GB002402.

Martin, J. H., et al. (1991), Testing the iron hypothesis in ecosystems of the equatorial Pacific Ocean, *Nature*, *371*, 123–129.

McPhaden, M. J. (2008), Evolution of the 2006–2007 El Niño: the role of intraseasonal to interannual time scale dynamics, *Adv. Geosci.*, *14*, 219–230.

Measures, C. I., J. J. Yang, L. J. Kaupp, L. T. Leonard, and G. M. Henderson (2006), Trace metal enrichments and their sources in the Equatorial Undercurrent of the central and eastern Pacific, *Geophys. Res. Abstr.*, *8*, 06155.

Measures, C. I., W. M. Landing, M. T. Brown, and C. S. Buck (2008a), A commercially available rosette system for trace metal clean sampling, *Limnol. Oceanogr. Methods*, *6*, 384–394.

Measures, C. I., W. M. Landing, M. T. Brown, and C. S. Buck (2008b), High-resolution Al and Fe data from the Atlantic Ocean CLIVAR-CO_2 Repeat Hydrography A16N: Extensive linkages between atmospheric dust and upper ocean geochemistry, *Global Biogeochem. Cycles*, *22*, GB1005, doi: 10.1029/2007GB003042.

Meehl, G. A., and W. M. Washington (1996), El Niño-like climate change in a model with increased atmospheric CO_2 concentrations, *Nature*, *382*, 56–60.

Menkes, C., J. G. Vialard, S. C. Kennan, J.-P. Boulanger, and G. V. Madec (2006), A Modeling Study of the Impact of Tropical Instability Waves on the Heat Budget of the Eastern Equatorial Pacific, *J. Phys. Oceanogr.*, *36*, 847–865.

Milliman, J. D., K. L. Farnsworth, and C. S. Albertin (1999), Flux and fate of fluvial sediments leaving large islands in the East Indies, *J. Sea Res.*, *41*, 97–107.

Moore, J. K., and O. Braucher (2008), Sedimentary and mineral dust sources of dissolved iron to the world ocean, *Biogeosciences*, *5*, 631–656.

Moore, J. K., S. C. Doney, and K. Lindsay (2004), Upper ocean ecosystem dynamics and iron cycling in a global three-dimensional model, *Global Biogeochem. Cycles*, *18*, GB4028, doi:10.1029/2004GB002220.

Murray, J. W., R. T. Barber, M. R. Roman, M. P. Bacon, and R. A. Feely (1994), Physical and biological controls on carbon cycling in the equatorial Pacific, *Science*, *266*, 58–65.

Nameroff, T. J. (1996), *Suboxic trace metal geochemistry and paleo-record in continental margin sediments of the eastern tropical north Pacific*, Ph.D. thesis, University of Washington.

Nishioka, J., et al. (2007), Iron supply to the western subarctic Pacific: Importance of iron export from the Sea of Okhotsk, *J. Geophys. Res.*, *112*, C10012, doi:10.1029/2006JC004055.

Obata, H., H. Karatani, and E. Nakayama (1993), Automated determination of iron in seawater by chelating resin concentration and chemiluminescence detection, *Anal. Chem.*, *65*, 1524–1528.

Orians, K. J., and K. W. Bruland (1986), The biogeochemistry of aluminum in the Pacific Ocean, *Earth Planet. Sci. Lett.*, *78*, 397–410.

Pakhomova, S. V., P. O. J. Hall, M. Y. Kononets, A. G. Rozanov, A. Tengberg, and A. V. Vershinin (2007), Fluxes of iron and manganese across the sediment-water interface under various redox conditions, *Mar. Chem.*, *107*, 319–331.

Philander, S. G. H. (1990), *El Nino and the southern oscillation*, Academic, San Diego, Calif.

Qu, T., S. Gao, I. Fukumori, R. A. Fine, E. J. Lindstrom (2009), Origin and pathway of equatorial 13°C water in the Pacific identified by a simulated passive tracer and its adjoint, *J. Phys. Oceanogr.*, *39*, 1836–1853.

Resing, J. A., and C. I. Measures (1994), Fluorometric determination of Al in seawater by flow injection analysis with in-line preconcentration, *Anal. Chem.*, *66*, 4105–4111.

Resing, J. A., and M. J. Mottl (1992), Determination of manganese in seawater by flow injection analysis using preconcentration and spectrophotometric detection, *Anal. Chem.*, *64*, 2682–2687.

Rodgers, K. B., B. Blank, G. Madec, O. Aumont, P. Ciais, and J.-C. Dutay (2003), Extratropical sources of equatorial Pacific upwelling in an OGCM, *Geophys. Res. Lett.*, *30*(2), 1084, doi:10.1029/2002GL016003.

Ryan, J. P., I. Ueki, Y. Chao, H. Hang, P. S. Polito, and F. P. Chavez (2006), Western Pacific modulation of large phytoplankton blooms in the central and eastern equatorial Pacific, *J. Geophys. Res.*, *111*, G02013, doi:10.1029/2005JG000084.

Severmann, S., J. McManus, W. M. Berelson, and D. E. Hammond (2010), The continental shelf benthic iron flux and its isotope composition, *Geochim. Cosmochim. Acta*, *74*, 3984–4004.

Shaked, Y., A. B. Kustka, and F. M. M. Morel (2005), A general kinetic model for iron acquisition by eukaryotic phytoplankton, *Limnol. Oceanogr.*, *50*(3), 872–882.

Shank, L. M., and A. M. Johansen (2008), Atmospheric trace metal and labile iron deposition fluxes to the equatorial Pacific during EUCFe2006, Ocean Sciences Meeting, Orlando, Fla, USA.

Sholkovitz, E. R., H. Elderfield, R. Szymczak, and K. Casey (1999), Island weathering: river sources of rare earth elements to the western Pacific Ocean, *Mar. Chem.*, *68*, 39–57.

Slemons, L. O., J. W. Murray, T. Gorgues, O. Aumont, and C. Menkes (2009), Biogeochemical impact of a model western iron source in the Pacific Equatorial Undercurrent, *Deep-Sea Res. Part I*, doi:10.1016/j.dsr.2009.08.005.

Sloyan, B. M., G. C. Johnson, and W. S. Kessler (2003), The Pacific cold tongue: A pathway for interhemispheric exchange, *J. Phys. Oceanogr.*, *33*.

Stoens, A., C. Menkes, Y. D. Radenac, N. Grima, G. Eldin, L. Mémery, C. Navarett, J. André, T. Moutin, and P. Raimbault (1999), The coupled physical-new production system in the equatorial Pacific during the 1992–1995 El Niño, *J. Geophys. Res.*, *104*(C2), 3323–3339.

Sunda, W. G., and D. G. Huntsman (1995), Iron uptake and growth limitation in oceanic and coastal phytoplankton, *Mar. Chem.*, *50*, 189–206.

Toggweiler, J. R., and S. Carson (1995), What are the upwelling systems contributing to the ocean's carbon and nutrient budgets?, in *Upwelling in the Ocean: Modern Processes and Ancient Records*, edited by C. P. Summerhayes et al., pp. 337–360, Wiley, New York.

Tsuchiya, M., R. Lukas, R. Fine, E. Firing, and E. Lindstrom (1989), Source waters of the Pacific equatorial undercurrent, *Prog. Oceanogr.*, *23*, 101–147.

Ueki, I., Y. Kashino, and Y. Kuroda (2003) Observation of current variations off the New Guinea coast including the 1997–1998 El Niño period and their relationship with sverdrup transport, *J. Geophys. Res.*, *108*(C7), 3243, doi:10.1029/2002JC001611.

Wells, M. L., G. K. Vallis, and E. A. Silver (1999), Tectonic processes in Papua New Guinea and past productivity in the eastern equatorial Pacific Ocean, *Nature*, *398*, 601–604.

Wu, J., E. Boyle, W. Sunda, and L. Wen (2001), Soluble and colloidal iron in the oligotrophic North Atlantic and North Pacific, *Science*, *293*, 847–849.

Yang, R., G. Henderson, J. C. M. de Hoog, and C. Measures (2009), Tracing sources of Fe to the central and eastern equatorial Pacific with rare earth elements and aluminum, *Goldschmidt 2009*, Abstract A147.

P. Dutrieux, British Antarctic Survey, Natural Environment Research Council, High Cross, Madingley Rd., Cambridge, CB3 0ET UK.

J. W. Murray, B. Paul, and L. O. Slemons, School of Oceanography, University of Washington, Box 355351, Seattle, WA 98195, USA. (ossianla@u.washington.edu)

J. Resing, Pacific Marine Environmental Laboratory, National Oceanic Atmospheric Administration, 7600 Sand Point Way NE, Seattle, WA 98115, USA.